A Consistent Bending Model for Cloth Simulation with Corotational Subdivision Finite Elements

Bernhard Thomaszewski, Markus Wacker, Wolfgang Straßer

Graphisch-Interaktive Systeme
Wilhelm-Schickard-Institut
Universität Tübingen
D-72076 Tübingen, Germany
e-mail: {thomaszewski, wacker, strasser}@gris.uni-tuebingen.de
WWW: http://www.gris.uni-tuebingen.de

Abstract

Modelling bending energy in a consistent way is decisive for the realistic simulation of cloth. With existing approaches characteristic behaviour like folding and buckling cannot be reproduced in a physically convincing way. We present a new method based on a corotational formulation of subdivision finite elements. Due to the non-local nature of the employed subdivision basis functions a C^1-continuous displacement field can be defined. It is thus possible to use the governing equations of thin shell analysis leading to a physically accurate bending behaviour. Using a corotated strain tensor allows the large displacement analysis of cloth while retaining a linear system of equations. Hence, known convergence properties and computational efficiency are preserved.

1   Introduction

Physically-based modelling has become the de facto standard in cloth simulation. For dynamically deformable surfaces, mass-spring systems continue to be the most widely used simulation technique in computer graphics. The popularity of this approach is due to the computational efficiency and easy implementation. While these methods already provide some parameters with physical interpretation like spring stiffness or damping coefficient they still incorporate important drawbacks when it comes to accurately reproducing specific material behaviours. Because of the inherent discretisation dependence homogeneous materials cannot be simulated consistently. Moreover, modelling volume conservation or transverse contraction is not possible without using further non-physical forces.

For authentic material mapping and hence realistic and reliable draping behaviour of cloth, as required e.g. by the textile community, one must necessarily resort to continuum mechanics. Techniques from this field are known to be computationally more expensive since they usually require the numerical solution of partial differential equations systems. When the first methods based on continuum mechanics were introduced to computer graphics (see e.g. Terzopoulos [TPBF87]) this was an essential disadvantage. However, with growing computational power available these solutions al-

low simulation at interactive rates even on standard PC hardware. The advantages offered by these methods are manifold: material behaviour can be reproduced accurately and independent from discretisation throughout a broad range of resolutions. Since these approaches originate from engineering sciences, tools and techniques from the thoroughly studied field of computational mechanics can be exploited. Generally speaking, each continuum formulation results in a set of partial differential equations (PDEs). Subsequently, this system has to be discretised in space and time. The spatial discretisation is usually carried out by means of finite differences (FDM) or finite element methods (FEM). FDMs are usually faster and easier to implement but are essentially limited to rectangular discretisations. With FEMs these complications do not arise. While this approach is computationally more expensive, according to Hauth [Hau04] an efficient implementation leaves only a factor roughly between two and three. This, however, has to be weighted against the increased precision and versatility offered by the FEM in comparison to classical mass-spring systems. A competitive FEM implementation for cloth simulation was recently presented by Etzmuss et al. [EKS03] who used a linear plane-stress assumption in conjunction with a rotation invariant strain formulation.

While there has been some effort spent on precisely reproducing the in-plane forces, few existing models are concerned with an accurate and consistent way of modelling bending energy. Nevertheless, the characteristic folding and buckling behaviour of cloth highly depends on bending properties. The reason for these difficulties is, however, not a lack of physical basis. From the field of engineering, the thin plate equations are known to be an adequate approach to this problem. Although common to computer graphics from fair surface design or variational modelling [WW98] they have not yet been successfully applied to cloth simulation. This again is due to the fact that the associated minimisation problem includes 4th order derivatives with respect to the displacements. A corresponding finite element approach therefore requires a C^1-continuous displacement field. The main problem with this requirement is to guarantee continuity across elements which usually necessitates the use of additional variables (e.g. slopes). Recently, Cirak et. al. [COS00] elegantly solved

this problem through the introduction of subdivision basis functions to finite element analysis. By applying these techniques to cloth simulation we obtain very fine detailed wrinkles as well as the typical folds appearing on sleeves of garments (cf. Figure 1). Hence, this is a promising way to incorporate the physical basis for bending models into the framework of cloth simulation with finite elements.

Figure 1: Different types of folds generated by our method illustrated on a fabric cylinder. *Left*: Catenary-shaped folds due to gravitational forces. *Middle*: Diagonal folds resulting from torsional deformation at one end. *Right:* Buckling due to compressive deformation.

2 Related Work

Cloth Simulation Throughout the last two decades there has been a lot of interest in cloth simulation and animation. A complete discussion of the relevant work is, however, beyond the scope of this paper and the reader is therefore referred to the textbook by House and Breen [HB00] or the overview compiled by Ng and Grimsdale [NG96] and Volino et al. [VCMT05].

In the following, we classify the previous work relevant to the presented approach into different categories.

FEM Finite element methods have not seen much attention in cloth simulation – at least not in computer graphics. Most of the existing approaches are based on the geometrically exact thin shell formulation presented by Simo et al. [SFR89]. Eischen [EDC96] departs from the fully nonlinear theory and applies it to cloth simulation using quadrilateral, curvilinear elements. A Newton-Raphson procedure is used to solve the resulting nonlinear equations. Because of the buckling behaviour of cloth which can lead to divergence in the algorithm an adaptive arc-length control is used. A different approach is taken by Etzmuss

et al. [EKS03] who presented a linear finite element approach based on a plane-stress assumption. Bending is treated separately from in-plane deformation while a corotational strain formulation is used to account for arbitrary rigid body transformations. The resulting equation system is solved using an efficient implicit time integration scheme. Cirak et al. [COS00] use the formulation of [SFR89] to derive equilibrium equations. They introduce a new kind of element based on subdivision basis functions. Unlike former FE formulations C^1-continuity is ensured through the nonlocal nature of the element shape functions while retaining linearity in displacements. The method was later extended to the finite deformation range using nonlinear theory [CO01, GCSO99]. This approach which was originally intendend for static analysis is, along with extensions to dynamical problems, taken as a basis for this work.

Corotational Formulation The extraction of the rotational part from the displacement field used in [EKS03] was already treated by Mller et al [MDM$^+$02] who used a warping heuristic. Using the geometry in the deformed state, local frames are computed per vertex and used to construct the rotations. However, due to the inaccuracy of this method occuring ghost forces have to be treated separately. A more precise method was presented by Hauth et al. [HS04] who used the polar decomposition of the deformation gradient. While the latter work proposes an interative solution for the 3D case, Etzmuss et al. use a direct approach for the simpler 2D problem. In our approach, the rotation field is extracted in a way similar to [EKS03], allowing stable treatment of arbitrarily large rigid body transformations.

Bending Models Most of the existing cloth simulation techniques use an angular expression to model bending energy or forces. Breen et al. [BHW94] use the linear beam theory relating bending moment to curvature. Curvature is approximated by fitting a circle to the three points defined by two incident edges. A biphasic expression in terms of the enclosed angle is then used for approximation. Volino et al. [VCMT95] use a similar approach but rely on the dihedral angle formed by two neighbouring triangles. Bridson et

al. [BMF03] identify an independent bending mode that is required to not affect rigid body transformations and in-plane deformations. The directions and relative magnitudes for a basic bending element consisting of two neighbouring triangles are thus derived. Grinspun et al. [GH+03] use a discrete mean curvature approximation for a sound definition of bending energy for flexible shell-like objects. Because the gradient computation is intricate the use of automatic differentiation is suggested. Choi and Ko [CK02] propose a bending model simultaneously accounting for compression and buckling. Specific assumptions on the post-buckling state and associated energy lead to the derivation of bending forces.

In this work, bending energy is modelled using the sound physical formulation of thin shell equations. Instead of artificially separating bending from membrane behaviour, deformation is treated consistently.

2.1 Overview and Contributions

In this paper we present an approach to cloth simulation which models both membrane and bending energy in a consistent way. The physical basis for this method are the Kirchhoff-Love thin shell equations which essentially combine the theory of elastic membranes with the Kirchhoff thin plate analysis. The approach proposed by Cirak et al. is extended to account for arbitrary rigid body transformations. Through the use of a corotational strain formulation this is achieved while preserving the linearity of the approach and thus retaining the associated advantages in convergence and computational efficiency. In addition, we present a simple method to incorporate various boundary conditions in the context of an implicit numerical solver.

3 Physical and Mathematical Modelling

In this section we will briefly describe the physical and mathematical background necessary for an understanding of our method. Throughout the remainder of this work Greek indices will take the values 1 and 2, Latin indices range from 1 to 3 and a comma denotes partial differentiation. Additionally, the summation convention is assumed [Bar89].

3.1 Notions from Continuum Mechanics

A deformable solid in its current state is described by its configuration mapping

$$\varphi : \Omega \to \mathbf{R}^3 \ , \tag{1}$$

where $\Omega \subseteq \mathbf{R}^3$ is its parameter domain. It is common to write this in terms of the rest state $\bar{\varphi}$ and a displacement field u as

$$\varphi = \bar{\varphi} + u = id + u \ , \tag{2}$$

where in the latter equation we assumed that the rest state mapping is simply the identity. Let $\bar{\mathbf{v}}_1 \cdot \bar{\mathbf{v}}_2$ be the scalar product of two elemental vectors $\bar{\mathbf{v}}_i = \bar{\mathbf{p}}_i - \bar{\mathbf{q}}$ in the rest state. Note that these vectors are related to their counterparts in the current configuration via

$$\varphi(\bar{\mathbf{v}}_i) = \varphi(\bar{\mathbf{p}}_i) - \varphi(\bar{\mathbf{q}}) \ . \tag{3}$$

A general deformation measure can now be derived as the difference of scalar products in the rest and current state:

$$\mathbf{v}_1 \cdot \mathbf{v}_2 - \bar{\mathbf{v}}_1 \cdot \bar{\mathbf{v}}_2 = \bar{\mathbf{v}}_1 \cdot (\nabla \varphi^T \nabla \varphi - \mathrm{id}) \bar{\mathbf{v}}_2. \tag{4}$$

Using eq. (2) we can identifiy from eq. (4) the symmetric Green strain tensor as

$$\begin{aligned} \varepsilon_G &= \frac{1}{2}(\nabla \varphi^T \nabla \varphi - id) \\ &= \frac{1}{2}(\nabla u^T + \nabla u + \nabla u^T \nabla u) \ . \end{aligned} \tag{5}$$

To investigate the internal forces related to a state of strain inside a deformable solid we let Π denote its total energy

$$\Pi = U + W \tag{6}$$

with elastic strain energy U and potential energy W due to applied forces. The strain energy is given in terms of the displacement field u as

$$U = \int_{\Omega} \varepsilon(u) : \sigma(u) \ d\Omega \ , \tag{7}$$

where σ is the symmetric *Cauchy stress* tensor which is related to strain through a material law as

$$\sigma = C(\varepsilon) \ . \tag{8}$$

In stable elastic equilibrium situations the total energy must be at a minimum [ZT00]. Mathematically, this can be reformulated by setting the first varitation of energy to zero, i.e. $\delta\Pi = 0$, which yields the virtual work equation:

$$\int_\Omega \delta\varepsilon : C(\varepsilon)d\Omega - \int_\Omega \delta u\ f\ d\Omega$$
$$+ \int_\Omega \delta u\ \rho\ \ddot{u}\ d\Omega = 0\ ,\quad (9)$$

where the last term on the left hands side accounts for inertial forces. This equation constitutes the basis for the subsequent finite element discretisation.

3.2 Kirchhoff-Love Thin Shell Equations

We will now provide a quick glance at the Kirchhoff-Love shell theory. For a detailed discussion of the mechanics of thin shells the reader is generally referred to [WT03, COS00, SFR89]. If no explicit reference is made, analogous formulation of the following equations are assumed for the initial configuration, too.

In the Kirchhoff-Love theory of thin shells the configuration mapping (1) is expressed in terms of the mid-surface parametrisation $\mathbf{x}(\theta^1, \theta^2)$ (see Figure 2) as

$$\varphi(\theta^1, \theta^2, \theta^3) = \mathbf{x}(\theta^1, \theta^2) + \theta^3 \mathbf{a}_3(\theta^1, \theta^2)\ ,\quad (10)$$

where θ^i denote curvilinear coordinates and $\mathbf{a}^3$ is the director field normal to the surface. In analogy to eq. (2) we write

$$\mathbf{x}(\theta^1, \theta^2) = \bar{\mathbf{x}}(\theta^1, \theta^2) + \mathbf{u}(\theta^1, \theta^2)\ .\quad (11)$$

From this, tangential surface basis vectors can be defined as

$$\mathbf{a}_\alpha = \mathbf{x}_{,\alpha}\ .\quad (12)$$

Moreover, the covariant tangent base vectors are given through differentiation of the configuration mapping as

$$\mathbf{g}_\alpha = \varphi_{,\alpha} = \mathbf{a}_\alpha + \theta^3 \mathbf{a}_{3,\alpha}\quad (13)$$

from which the surface *metric tensor* is derived as

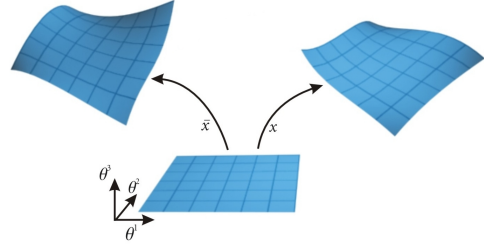$$g_{ij} = \mathbf{g}_i \cdot \mathbf{g}_j.\quad (14)$$

Figure 2: The shell's mid-surface in its reference, initial, and current configuration.

Following eq. (5) this leads to the definition of the Green strain

$$\varepsilon_{ij}^G = \frac{1}{2}(g_{ij} - \bar{g}_{ij}) = \alpha_{ij} + \theta^3 \beta_{ij}\ ,\quad (15)$$

where α and β are membrane and bending strains, respectively. In the Kirchhoff-Love theory, the director $\mathbf{a}_3$ is assumed to stay normal to the surface, straight and unstretched:

$$\mathbf{a}_3 = \frac{\mathbf{a}_1 \times \mathbf{a}_2}{|\mathbf{a}_1 \times \mathbf{a}_2|}\ .\quad (16)$$

Consequently, we have $\alpha_{3\beta} = \alpha_{\alpha3} = 0$. The strains then simplify to

$$\alpha_{\alpha\beta} = \frac{1}{2}(\mathbf{a}_\alpha \cdot \mathbf{a}_\beta - \bar{\mathbf{a}}_\alpha \cdot \bar{\mathbf{a}}_\beta)$$
$$\beta_{\alpha\beta} = (\bar{\mathbf{a}}_{\alpha,\beta} \cdot \bar{\mathbf{a}}_3 - \mathbf{a}_{\alpha,\beta} \cdot \mathbf{a}_3)\ .$$

Departing from $\mathbf{a}_\alpha = \mathbf{x}_{,\alpha} + \mathbf{u}_{,\alpha}$ and neglecting nonlinear terms, this can be recast to an expression which is linear in displacements [COS00, eq.(21),(22)]. Resultant membrane and bending stresses follow as

$$n^{\alpha\beta} = \frac{\partial\Psi}{\partial\alpha_{\alpha\beta}}\ ,\quad m^{\alpha\beta} = \frac{\partial\Psi}{\partial\beta_{\alpha\beta}}\ ,\quad (17)$$

where Ψ is the strain energy density. The particular form of Ψ depends on the material law used. In this work we used a linear isotropic stress-strain relationship which leads to

$$\sigma = \mathcal{C}\varepsilon\ ,\quad (18)$$

where $\mathcal{C}$ can be written in terms of the Lam coefficients λ and μ as $\mathcal{C}_{ijkl} = \lambda\delta_{ij}\delta_{kl} + 2\mu\delta_{ik}\delta_{jl}$.

4

3.3 Strain measures

Introducing the deformation gradient F as

$$F = \frac{\partial \varphi}{\partial \bar{\varphi}}$$

eq. (5) can be alternatively written in the form

$$\varepsilon^G = \frac{1}{2}(F^T F - id) \qquad (19)$$

(see [BW97]). Via polar decomposition F can be split into a rotational part R and a pure deformation U as $F = RU$. From this, it can be seen that ε^G is invariant under rotations since

$$F^T F = U^T R^T R U = U^T U \qquad (20)$$

due to the orthogonality of R. The linearisation of the Green strain tensor ε^G yields the *Cauchy* strain tensor

$$\varepsilon^C = \frac{1}{2}(\nabla u^T + \nabla u). \qquad (21)$$

This tensor is linear in displacements but not rotationally invariant any more. However, if the rotation field R is known, the corotational strain formulation can be used and we obtain the rotated linear strain tensor:

$$\varepsilon^{CR}(\varphi) = \varepsilon^{CR}(R^T \varphi). \qquad (22)$$

How to determine this rotation field is crucial for our calculation and will therefore be detailed in section 4.3.

4 Subdivision-Based Finite Elements

This section explains how to construct the subdivision-based finite element solution of the virtual work equation (9). Although well known to computer graphics, the concept of subdivision is briefly recapitulated before we proceed to the actual discretisation. The extraction of rotations from the displacement field is detailed subsequently and finally, the incorporation of boundary conditions is discussed.

4.1 Subdivision Surfaces

Subdivision is a process for constructing smooth limit surfaces through successive refinement of an initial control mesh. Basically, this procedure consists of two steps: first, the geometry is refined through introduction of new nodes and second, new nodal positions are computed. For a discussion of the diversity of subdivision schemes the reader is referred to [ZS00] for an overview. Here, we limit our attention to Loop's subdivision scheme which was also used by Cirak et al [COS00]. Loop's scheme is approximating, i.e. the nodes of the mesh at a coarser level are not contained in meshes at finer levels. However, besides the usual C^1-continuity inherent to subdivision surfaces the curvature is L_2- or square integrable [RS00] – a feature not offered by interpolating schemes. Because of this property, the subdivision basis functions can be used as shape functions for the FE solution of the thin shell equations. In each step of this subdivision method, the positions of newly inserted nodes as well as those of old nodes are computed through a linear combination of vertices from the coarse mesh determined by the so called subdivision mask. In the case of Loop
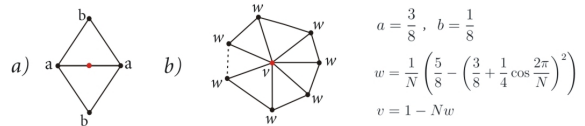

Figure 3: Subdivision masks: *a)* Edge mask to determine new vertex. *b)* Mask for vertex with valence N.

subdivision only the immediate neighbours (i.e. the 1-ring) of a vertex have influence on this computation which gives rise to efficient implementation. The corresponding vertex masks for computing the new positions are shown in Figure 3. The subdivision process can be considered as a linear operator and consequently be written in matrix form. It is therefore possible to directly derive properties like derivatives of the limit surface using an Eigenanalysis of the subdivision matrix. This yields simple expressions that can be computed efficiently (see Figure 4). Besides the evaluation at the nodes these quantities can also be determined at the interior of the triangulation. The key observation is that in regular settings (i.e. when the involved vertices all have valence 6) Loop's scheme leads to generalised
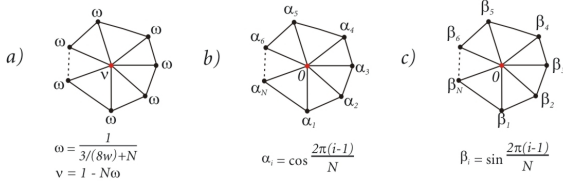
Figure 4: *a)*: Limit mask for a vertex of valence N. *b) and c)*: Masks for associated tangent vectors.

quartic box splines. In this case surface porperties in one triangle (or *patch*) are completely defined through the 12 nodal values in the 1-neighbourhood (see Figure 5) and the associated box spline basis functions N_i. For instance, if we denote by θ^α the
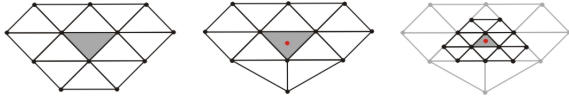

Figure 5: *Left*:1-neighbourhood of a regular patch consisting of 12 nodes. *Middle*: Irregular patch with one vertex of valence 5. *Right*: After a single local sudivision step the barycenter (depicted in red) lies again in a regular neighbourhood.

local patch coordinates, the limit surface can be expressed as

$$\mathbf{x}(\theta^1, \theta^2) = \sum_i^{12} N_i(\theta^1, \theta^2)\mathbf{x}_i , \qquad (23)$$

where $\mathbf{x}_i$ are the nodal positions of the underlying mesh. In the same way, the displacement field interpolation is obtained from the nodal values. Additionally, differential quantities can be determined as

$$\mathbf{x}_{,\alpha}(\theta^1, \theta^2) = \sum_i^{12} N_{i,\alpha}(\theta^1, \theta^2)\mathbf{x}_i . \qquad (24)$$

If the patch has an irregular vertex the box spline assumption no longer holds and thus interior parameter points cannot be evaluated. However, since a subdivision step does not alter the properties of the limit surface, we can simply apply further subdivision steps until the point of interest lies inside a regular patch. We point out that for the following finite element scheme only quantities at the barycenter of the triangles are needed for integral evaluation. Furthermore, if we require that in the initial mesh there is at most one irregular vertex per triangle, one subdivision step is always sufficient

because, thereafter, the barycenter of the irregular patch lies in a regular subpatch (see Figure 5). This process of subdivision and evaluation of the newly generated patch can again be expressed as a sequence of matrix multiplications. Though sufficient for this case, the presented method could be extended to quantity evaluation at arbitrary parameter values using the technique proposed by Stam [Sta99].

With this powerful interpolation scheme at hand we can now proceed to the actual finite element discretisation.

4.2 Spatial Discretisation

The spatial discretisation of the underlying PDE has been described in detail by Cirak et al. [COS00]. For completeness, we simply mention the relevant formulae and refer the interested reader to the original work.

With the definition of the membrane and bending strains and assuming a linear elastic material (eq. (18)) the internal energy from eq. (9) can be rewritten as

$$\int_\Omega \delta\varepsilon : C(\varepsilon)d\Omega = $$
$$\int_\Omega \left(\delta\alpha^T \mathbf{H}_m \alpha + \delta\beta^T \mathbf{H}_b \beta \right) d\Omega , \quad (25)$$

where $\mathbf{H}_m$ and $\mathbf{H}_b$ are matrices corresponding to the membrane and bending part of the material law. Due to the linear strain interpolation, we have

$$\alpha(\theta^1, \theta^2) = \sum_i^N \mathbf{M}_i(\theta^1, \theta^2)\mathbf{u}_i,$$
$$\beta(\theta^1, \theta^2) = \sum_i^N \mathbf{B}_i(\theta^1, \theta^2)\mathbf{u}_i$$

for matrices $\mathbf{M}_i$ and $\mathbf{B}_i$ relating nodal displacements $\mathbf{u}_i$ to membrane and bending strain. This gives rise to a formulation of the complete system in the classical form of

$$\mathbf{Ku} = \mathbf{f} \qquad (26)$$

with vectors of nodal displacement $\mathbf{u}$ and forces $\mathbf{f}$. The stiffness matrix $\mathbf{K}$ can be assembled in the

usual element-wise fashion

$$\mathbf{K}_{ij} = \sum_e \int_{\Omega_e} \left(\mathbf{M}_i^T \mathbf{H}_m \mathbf{M}_j + \mathbf{B}_i^T \mathbf{H}_b \mathbf{B}_j \right) d\Omega$$

$$= \sum_e \mathbf{K}_{ij}^e \ . \tag{27}$$

We point out that due to the compact support of the shape functions, only a finite number of elements have a non-zero contribution to $\mathbf{K}_{ij}$. This leads to a sparse matrix system for which efficient solvers are available. Moreover, the integrals in eq. (27) can be evaluated using numerical quadrature. Although more accurate schemes are possible, we follow Cirak et al. and use a one-point quadrature rule at the center of the triangles. As they are, the above equations are only valid on regular patches. However, as mentioned above, in irregular settings one subdivision step is sufficient for evaluations at the barycenters. For a patch with irregular vertex of valence N let $\mathbf{S}$ denote the $((N + 12) \times (N + 6))$-matrix of the subdivision operator which transforms the $N + 6$ vertices of the original patch to the corresponding $N + 12$ vertices of the subdivided patch (see [COS00]). Further, let $\mathbf{P}$ be the $(12 \times (N + 12))$ matrix of the projection operator extracting the 12 vertices corresponding to the central regular subpatch (Figure 5, right). Then we can write

$$\mathbf{K}_{ij}^e = \int_{\Omega_e} \left[\mathbf{S}^T \mathbf{P}^T \left(\mathbf{M}_i^T \mathbf{H}_m \mathbf{M}_j + \mathbf{B}_i^T \mathbf{H}_b \mathbf{B}_j \right) \mathbf{P} \mathbf{S} \right] d\Omega$$

and thus simply include the conceptual subdivision step into the stiffness matrix.

For dynamical reasons inertial as well as viscous forces have to be included which leads to the second order ODE

$$\Lambda \ddot{\mathbf{u}}_n + \mathbf{D} \dot{\mathbf{u}}_n + \mathbf{K} \mathbf{u} = \mathbf{f} \ , \tag{28}$$

where Λ is the diagonal nodal mass matrix obtained via mass lumping and $\mathbf{D}$ is the viscosity matrix. We use a viscous tensor proportional to the elasticity tensor, $\mathcal{D} = \nu \mathcal{C}$, which is derived from a Kelvin-Voigt material model [HGS03]. For the numerical solution, eq. (28) is transformed into a set of coupled first order ODEs. The implicit time integration is then carried out using a conjugate gradient scheme with the nodal velocities as primary unknowns (see e.g. [EKS03]).

4.3   Corotational Formulation

Provided the deformations stay small throughout the simulation they can be approximated using a linear displacement formulation. While this is a reasonable assumption for the in-plane deformation (i.e. stretching and shearing) of cloth, any practical application will most likely lead to large bending deformations and rigid body transformations, including rotation. Since the Cauchy strain is not rotationally invariant, one has to extract the rotations from the displacement field as already mentioned in eq. (22). This paragraph describes this process using a polar decomposition of the deformation gradient F.

With the definition of the configuration mapping (10) the deformation gradient can be written as

$$F = \frac{\partial \varphi}{\partial \bar{\varphi}} = \frac{\partial \varphi}{\partial \theta^i} \otimes \bar{\mathbf{g}}^i = \left[\mathbf{a}_\alpha + \theta^3 \mathbf{a}_{3,\alpha} \right] \otimes \bar{\mathbf{g}}^\alpha + \mathbf{a}_3 \otimes \bar{\mathbf{g}}^3 \ ,$$

where $\bar{\mathbf{g}}^i$ are the contravariant basis vectors which are related to their covariant counterparts via $\bar{\mathbf{g}}^i \cdot \bar{\mathbf{g}}_j = \delta_{ij}$ (see [WT03]). In this form, the deformation gradient is a (3×3)-tensor and its polar decomposition would necessitate the use of an iterative scheme [HS04]. In our case, we want to further exploit the inherent two-dimensionality of the problem. The assumed kinematic restrictions on the shell (i.e. that the director remains straight, normal and unstretched) effectively render the decomposition problem two-dimensional since we have for the resulting stretch tensor

$$\mathbf{U} = \begin{bmatrix} U_{11} & U_{12} & 0 \\ U_{12} & U_{22} & 0 \\ 0 & 0 & 1 \end{bmatrix} \ . \tag{29}$$

From eq. (20) we can thus deduce that only the (2×3)-submatrix $\tilde{\mathbf{F}}$ will be relevant for the computation of $\mathbf{U}^2$. We therefore compute the principal stretches in the 2D subspace and find the rotation $\tilde{\mathbf{R}}$ which transforms the element from the initial (flat) configuration to its current position by

$$\tilde{\mathbf{R}} = \tilde{\mathbf{F}} \tilde{\mathbf{U}}^{-1} \ , \tag{30}$$

where $\tilde{\mathbf{U}}$ is the upper (2×2) submatrix of $\mathbf{U}$.

In the presented approach, the deformation gradient is not constant over an element and thus, theoretically, rotations might be different for each vertex. However, we found that using the rotation

obtained for the barycenter of the patch for all the vertices involved was sufficient in all of our tests. Only in the case of very inhomogeneous deformation this might lead to noticeabe approximation errors which, again, did not appear in practice.

4.4 Boundary Conditions

The evaluation of integrals (appearing in equation (27)) for elements on the border of the domain requires special versions of the subdivision rules. To avoid the treatment of these special cases Cirak et al. suggest the use of a method proposed by Schweitzer [Sch96] which consists in introducing a layer of artificial vertices around the boundary. The positions of these vertices are calculated from their original neighbours such that the application of the normal subdivision rules effectively reproduces the behaviour of the border rules. When imposing boundary conditions, i.e. constraints on the boundary nodes, the artificial vertices have to be taken into account. The case of a fixed boundary with rotations allowed (simply supported) is depicted in Figure 6 (for an in depth discussion of boundary conditions see [GT04]). In this case
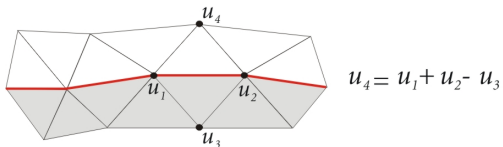

$$u_4 = u_1 + u_2 - u_3$$

Figure 6: Connectivity of an artificial vertex u_4 around the boundary (shown in red). The displacement of u_4 is determined by its local neighbours. In the example, the border is fixed while allowing rotations.

the displacements of both the artificial and the actual boundary vertices are constrained. However, the difference between these two vertex types is that the constraints of the boundary vertices are *fixed* while those imposed on the artificial vertices are linearly dependent on the input variables and thus *vary* when the latter change, too. Now, if the equation system arising from (28) is to be solved using an iterative scheme like the conjugate gradient method, this interdependence between the input variables actually hinders the convergence and might even lead to divergence. Fortunately, this inconvenience can be circumvented through elimination of the boundary vertices from the equation system. Clearly, simply erasing the corresponding rows and columns from the system matrix $\mathbf{K}$ would not be sufficient since the boundary conditions would thus be violated. The right choice is to *distribute* the columns corresponding to the artificial vertices to the columns associated with the original nodes. This is carried out through elemental matrix transformations, i.e. additions and subtractions of columns, that are guaranteed to neither change the solution of the system nor its behaviour. Through these manipulations, the resulting matrix is no more symmetric and has to be symmetrized by applying the same transformations to its rows. Once these adjustments have been made the system matrix can be projected onto the actual solution space determined by the displacements of the original vertices.

5 Results

In this section we present results obtained from our corotational subdivision-based finite element method for cloth simulation. In all of the examples, the visual quality resulting from the consistent bending model presented above can be seen. Figure 7 shows an example common for cloth simulation: a piece of cloth is fixed in space at two corners which have rotational degrees of freedom. It swings
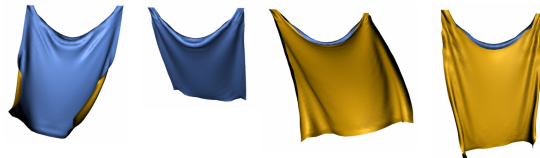

Figure 7: Snapshots from swinging cloth.

freely and exhibits folds due to both weight and inertial forces which correspond to the fixation at both ends of the cloth. Besides the usual dynamic test cases we additionally chose fabric cylinders as basic testing primitives. This is because cylindrical shapes are frequently encountered with clothes, e.g. the sleeves of a sweater can be reasonably approximated in this way. Thus, we have a method to investigate the quality of our approach with respect to static buckling and folding situations. We believe that the capability of modelling these kinds of features is decisive for any cloth simulation technique and we invite the reader to consider the results produced by our method (see Figure 1,8,9,11).

In addition to these basic experiments we validate our method through the application to standard clothes like a sweater or a pair of trousers.

In the first example, a fabric cylinder is subjected to gravitational loading and shows the expected catenary-shaped folds (see Figure 1, left). The cylinder is then wrung, showing distinct diagonal folds (Figure 1, middle) and finally compressed, neglecting forces due to gravitation (Figure 1, right). The specific folds expected in this situation are clearly reproduced by our method and we claim that very similar behaviour can be observed with real fabrics, such as the sleeves of a sweater. The geometric model used in this example consists of 900 faces and is, compared to the detail of the results, relatively coarse for standard cloth simulation.

The global shape of the results obtained from our simulation is undoubtably due to the consistent way of modelling bending energy. Using the Loop subdivision basis functions, it is possible to capture the deformation behaviour also at a more global scale while conventional methods are inherently limited to the bending interaction between single triangles or edges. If fine discretisations are used, the latter approaches can possibly account for small detailed wrinkles but often lack globally convincing appearance. The relative discretisation independency of our method can also be seen in Figure 8 where we have chosen different material parameters for fabric thickness and stretch resistance. It is interesting to note, that the number

Figure 8: Front view of twisted fabric cylinders made of different materials. *Left:* a thin, *middle:* a ten times thicker material. *Right:* as in the middle but with a ten times stronger stretch resistance. In all of the examples, the same mesh was used.

of diagonal folds appearing in consequence to the torsional deformation does obviously only depend on material parameters and not on the discretisation, since we used the same mesh in all three cases. In fact, this behaviour is not accidental but derives from the buckling properties of cylindrical

shells [AP04].

In Figures 9 and 11 some snapshots from animations we produced with our method are shown. Figure 11 depicts the axial compression of a cylinder while 9 shows a cylinder subjected to torsional deformation. In both examples, one can clearly no-

Figure 9: Torsional deformation of a cylinder.

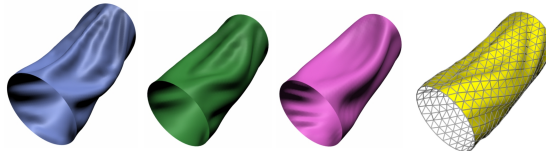tice the forming of folds starting with fine wrinkles which merge into bigger folds.

Figure 10: Fabric cylinders under gravitational loading with different material parameters. *Right*: Mesh used in computation.

Using different material parameters for the underlying elastic properties of the deformable objects consistently yields different deformation behaviour (see Figure 10). Compare for example the buckled shape shown in Figure 1 where we used material parameters corresponding to cotton-like cloth ($E \approx 5000N/m^2$) and the results depicted in Figure 11, where parameters leading to a behaviour similar to thin flexible metal were used ($\lambda = 10^6$). In the second part we verified our approach with
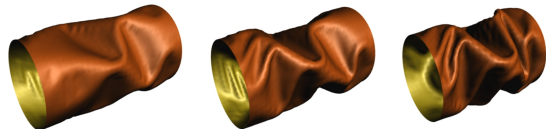

Figure 11: Sequence taken from an animation of axial compression of a cylinder

common garments suchs as a sweater or a pair of trousers. The trousers and the sweater consist of 1600, resp. 1000 vertices. Both are fixed at the ends of the extremities and are subjected to gravity (see Figure 12). Here, naturally appearing folds
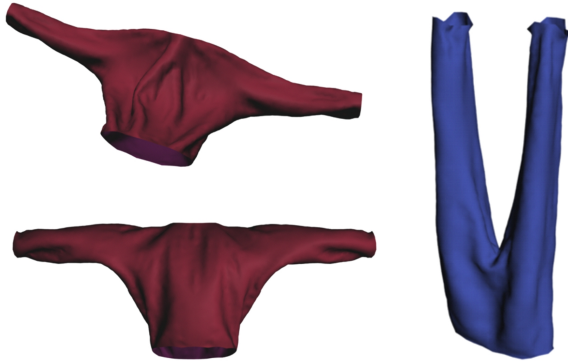
Figure 12: Sweater under gravitational loading, *Top left*: view from above and *Bottom left*: bottom view. *Right*: a pair of trousers pinned at the legs is hanging vertically.

and wrinkles are obtained and catenary folds as well as buckling patterns can be observed. Despite the rather coarse discretisation of the meshes used in this example detailed features and, at the same time, convincing global appearance can be reproduced without any need for post-processing or non-physical intervention.

6 Conclusion and Future Work

We have proposed a method for consistently modelling membrane and bending energies arising in the simulation of thin, flexible objects such as cloth. With the advent of subdivision-based finite elements, cloth simulation can now be founded on the physically sound basis of the thin shell equations. A novel achievement of the presented work is the combination of this new paradigm with a corotational strain formulation allowing for a completely linear system which, in turn, leads to efficient implementation. The presented examples clearly demonstrate the advantages of our method above previous approaches: when phenomena highly dependent on bending properties are encountered, like e.g. the buckling of fabric, usual methods fail without further non-physical intervention while our approach shows the expected behaviour. Furthermore, common post-processing steps can be integrated in a

very elegant way, if desired. Since the employed subdivision basis leads to smooth limit surfaces, the geometry can be locally evaluated and refined to the desired degree.

A limitation of the presented method which is, in fact, inherent to all applications based on approximating subdivision schemes is that the limit surface does not interpolate the vertices of the control mesh. Nevertheless, it may be doubted that the approximation of cloth as a piecewise linear surface is more sensible.

We believe that our method has strong arguments when it comes to trading accuracy for computational efficiency: while current computation times are certainly beyond the interactive range the physical fidelity and versatility offered by this method can be of great interest to anyone wishing to reproduce fabric behaviour in an accurate way.

To be really competitive with existing precise solutions a robust collision and interference detection scheme for subdivision surfaces is indispensable for future work (cf. [GS01]). A closer investigation of our solution combined with different material types is interesting, too. Finally, the application of multiresolution numerics is almost an obvious extension (cf. [GTS02]) which motivates expectations on a boost in computational efficiency.

7 Acknowledgements

References

[AP04]   K. Athiannan and R. Palaninathan. Experimental investigations on buckling of cylindrical shells under axial

10

compression and transverse shear. *Sadhana*, pages 93–115, February 2004.

[Bar89]   A. H. Barr.   The einstein summation notation: Introduction and extensions. *SIGGRAPH 89 Course Notes on Topics in Physically-Based Modeling*, 30:J1–J12, 1989.

[BHW94]   D. Breen, D. House, and M. Wozny. Predicting the drape of woven cloth using interacting particles. In *Proceedings of ACM SIGGRAPH 94*, pages 365–372. ACM Press, 1994.

[BMF03]   R. Bridson, S. Marino, and R. Fedkiw. Simulation of clothing with folds and wrinkles. In *Proceedings of ACM SIGGRAPH/Eurographics Symposium on Computer Animation (SCA 2003)*, pages 28–36. ACM Press, 2003.

[BW97]   J. Bonet and R. D. Wood. *Nonlinear Continuum Mechanics for Finite Element Analysis.* Cambridge University Press, 1997.

[CK02]   K.-J. Choi and H.-S. Ko. Stable but responsive cloth. *ACM Transactions on Graphics (ACM SIGGRAPH 2002)*, 21(3):604–611, July 2002.

[CO01]   F. Cirak and M. Ortiz.   Fully C^1-conforming subdivision elements for finite deformation thin-shell analysis. *Journal for Numerical Methods in Engineering*, 51:813–833, 2001.

[COS00]   F. Cirak, M. Ortiz, and P. Schröder. Subdivision surfaces: A new paradigm for thin-shell finite-element analysis, 2000.

[EDC96]   J. Eischen, S. Deng, and T. Clapp. Finite-element modeling and control of flexible fabric parts. *IEEE Computer Graphics and Applications*, 16(5):71–80, September 1996.

[EKS03]   O. Etzmuss, M. Keckeisen, and W. Straßer. A Fast Finite Element Solution for Cloth Modelling. *Proceedings of Pacific Graphics*, 2003.

[GCSO99]   E. Grinspun, F. Cirak, P. Schrder, and M. Ortiz.   Non-linear mechanics and collisions for subdivision surfaces. Technical report, Caltech Multi-Res Modeling Group, 1999.

[GH+03]   E. Grinspun, , A. Hirani, M. Desbrun, and P. Schröder.   Discrete shells. In *Proceedings of ACM SIGGRAPH/Eurographics Symposium on Computer Animation (SCA 2003)*, pages 62–67. ACM Press, 2003.

[GS01]   E. Grinspun and P. Schrder. Normal bounds for subdivision-surface interference detection, 2001.

[GT04]   S. Green and G. Turkiyyah. Second-order accurate constraint formulation for subdivision finite element simulation of thin shells. *International Journal for Numerical Methods in Engineering*, 61(3):380–405, 9 2004.

[GTS02]   S. Green, G. Turkiyyah, and D. Storti. Subdivision-based multilevel methods for large scale engineering simulation of thin shells. In *SMA '02: Proceedings of the seventh ACM symposium on Solid modeling and applications*, pages 265–272. ACM Press, 2002.

[Hau04]   M. Hauth.   Visual simulation of deformable models. Phd thesis, Wilhelm-Schickard-Institut für Informatik, University of Tübingen, Germany, July 2004.

[HB00]   D. H. House and D. E. Breen, editors. *Cloth modeling and animation.* A. K. Peters, Ltd., Natick, MA, USA, 2000.

[HGS03]   M. Hauth, J. Groß, and W. Straßer. Soft tissue simulation based on measured data. In *Proc. MICCAI*, 2003.

[HS04]   M. Hauth and W. Straßer. Corotational simulation of deformable solids. In *Proc. WSCG 2004*, pages 137–145, 2004.

[MDM+02]   M. Mller, J. Dorsey, L. McMillan, R. Jagnow, and B. Cutler.   Stable real-time deformations.   In *SCA*

'02: Proceedings of the 2002 ACM SIGGRAPH/Eurographics symposium on Computer animation, pages 49–54, New York, NY, USA, 2002. ACM Press.

[NG96]   H. N. Ng and R. L. Grimsdale. Computer graphics techniques for modeling cloth. *IEEE Comput. Graph. Appl.*, 16(5):28–41, 1996.

[RS00]   U. Reif and P. Schröder. Curvature integrability of subdivision surfaces. *Advances in Computational Mathematics*, pages 1–18, 2000.

[Sch96]   J. E. Schweitzer. Analysis and application of subdivision surfaces. Technical Report TR-96-08-02, 1996.

[SFR89]   J.C. Simo, D.D. Fox, and M.S. Rifai. On a stress resultant geometrically exact shell model. part i: Formulation and optimal parametrization. In *Comput. Methods Appl. Mech. Engrg.*, volume 72, pages 267–302, 1989.

[Sta99]   J. Stam. Evaluation of loop subdivision surfaces. In *SIGGRAPH '99 Course Notes*, 1999.

[TPBF87]   D. Terzopoulos, J. Platt, A. Barr, and K. Fleischer. Elastically deformable models. In *Computer Graphics (Proceedings of ACM SIGGRAPH 87)*, pages 205–214. ACM Press, July 1987.

[VCMT95]   P. Volino, M. Courchesne, and N. Magnenat-Thalmann. Versatile and efficient techniques for simulating cloth and other deformable objects. In *Proceedings of ACM SIGGRAPH 95*, pages 137–144. ACM Press, 1995.

[VCMT05]   P. Volino, F. Cordier, and N. Magnenat-Thalmann. From early virtual garment simulation to interactive fashion design. *Computer-Aided Design Journal, Elsevier*, 37:593–608, 2005.

[WT03]   G. Wempner and D. Talaslidis. *Mechanics of solids and shells: Theories and approximations*. CRC Press, 2003.

[WW98]   H. Weimer and J. Warren. Subdivision schemes for thin plate splines. *Computer Graphics Forum*, 17(3):303–314, 1998. ISSN 1067-7055.

[ZS00]   D. Zorin and P. Schröder. Subdivision for Modeling and Animation. In *SIGGRAPH '00 Course Notes*, 2000.

[ZT00]   O.C. Zienkiewicz and R.L. Taylor. *The Finite Element Method. Volume 1: The Basis*. Butterworth Heinemann, 5th edition, 2000.